Nonuniform broken-parity waves and the Eckhaus instability

Lihong Pan and John R. de Bruyn
Department of Physics, Memorial University of Newfoundland, St. John's, Newfoundland, Canada A1B 3X7
(Received 3 November 1993)

We report measurements on broken-parity traveling finger patterns which form at an oil-air interface driven by the rotation of two acentrically mounted horizontal cylinders. In the parameter region studied here, the wavelength, traveling speed, and degree of asymmetry of the traveling fingers vary along the interface. As our control parameter is increased, we observe a transition at which the average values of these properties suddenly decrease. The traveling patterns are intermittently interrupted by periods of disordered behavior, which become more frequent near this transition. The variation of wavelength along the pattern allows us to observe what appears to be the Eckhaus instability: outside a range of wavelengths, the drifting fingers become unstable, resulting in the birth of new fingers if the local wavelength is too long, or the disappearance of a finger if it is too short. We measure the Eckhaus stability boundary for this system.

PACS number(s): 47.20.Ky, 47.20.Lz, 47.54.+r, 68.10.Gw

I. INTRODUCTION

Instabilities in pattern-forming systems have been studied extensively in recent years [1]. In this paper, we report on some measurements on propagating one-dimensional patterns with broken parity symmetry [2–7]. The phenomenon of parity breaking has been studied in several well-known pattern-forming systems, including several variants of directional solidification [8–19], Taylor-Couette flow [20,21], and Taylor-Dean flow [22], as well as in the system studied here, which is known as the printer's instability [23–28]. In all of these systems, a stationary, one-dimensional pattern develops as the system is driven out of equilibrium by varying an experimental control parameter. This pattern is then subject to a secondary parity-breaking instability, where it loses its reflection symmetry, leading to a state in which the pattern travels [2,3].

In our experiments, a thin layer of oil fills the narrowest part of the gap between two horizontal cylinders, one mounted acentrically inside the other. The oil-air interface running the length of the cylinders is straight when they are at rest, but a pattern of fingers forms along the interface when it is driven by rotating the cylinders. The dynamical phase diagram of our experimental system is shown in Fig. 1. The two control parameters are v_i and v_o, the surface speeds of the rotating inner and outer cylinders, respectively. In the region labeled stable, the oil-air meniscus at the front of the apparatus is straight. In the regions labeled S, the straight interface is unstable to a pattern of stationary fingers [23,29,30]. In the regions labeled SW, solitary waves, consisting of localized patches of broken-parity fingers, propagate through the stationary finger pattern [23], and TW indicates a state in which the entire interface consists of asymmetric traveling fingers [23,26–28]. STC indicates a region where the pattern is spatiotemporally chaotic [31]. In our previous work on this system [27,28], we studied the traveling-wave state in the shaded portion of the TW region in the second quadrant of Fig. 1. In this region we found that, for a given, fixed value of the rotation speed of the outer cylinder, v_o, increasing v_i in the opposite direction (i.e., moving to the left along a horizontal line in Fig. 1) resulted in a supercritical bifurcation to the broken-parity traveling finger state. We showed that the pattern's traveling speed, as well as the degree of asymmetry of the pattern, were proportional to $(v_i - v_i^*)^{1/2}$, where v_i^* is the value of v_i at the onset of the parity-

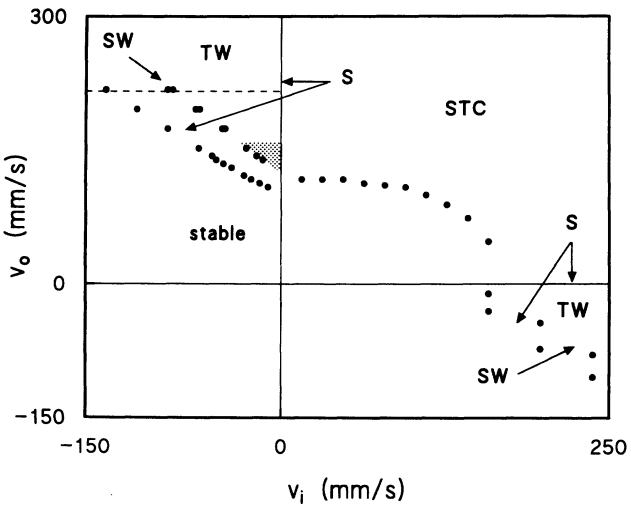

FIG. 1. The dynamical phase diagram of the interface, in terms of the rotation speeds, v_i and v_o, of the inside and outside cylinders. S: stationary fingers; TW: traveling waves; STC: spatiotemporal chaos; SW: solitary waves. The uniform broken-parity waves we studied in Refs. [27,28] exist in the shaded region of the second quadrant. The current experiments were done in the same TW region, but at higher v_o. A typical experimental path is shown by the dashed horizontal line.

breaking transition, and that the propagation speed was linearly related to the asymmetry.

Parity-breaking transitions in one-dimensional patterns have been studied theoretically by a number of groups. Coullet and co-workers developed a model based on coupled amplitude and phase equations, derived from simple symmetry arguments [2,4,5]. They split the pattern into parts which are even and odd with respect to reflections, writing

$$U(x) = SU_S(x+\phi) + AU_A(x+\phi). \tag{1}$$

Here U_S and U_A are even and odd functions of their arguments, respectively, x is the position variable along the pattern, and A, S, and ϕ are all assumed to vary slowly in space. The amplitude A of the antisymmetric term is taken as the order parameter of the parity breaking, and ϕ is the phase of the pattern relative to that of the underlying symmetric pattern. Taking into account the required symmetries of the pattern, it is straightforward to write down equations for the behavior of A and ϕ [2]:

$$A_t = A_{xx} + \mu A - A^3 + \epsilon\phi_x A + \cdots, \tag{2}$$

and

$$\phi_t = \phi_{xx} + \omega A + \cdots, \tag{3}$$

where we have assumed a supercritical parity-breaking bifurcation. μ is the control parameter, and ϵ and ω are unknown coupling constants. From these equations, assuming a spatially uniform pattern, we expect the pattern's asymmetry A to grow like

$$A = (\mu + \epsilon\phi_x)^{1/2}, \tag{4}$$

while the pattern's phase velocity, which is equal to ϕ_t, should be proportional to A:

$$v_\phi = \omega A. \tag{5}$$

Our previous measurements [27,28] were in agreement with these predictions.

Fauve and co-workers have studied the parity-breaking instability in terms of a specific model, involving the resonant coupling between spatial modes of wave numbers q and $2q$ [6,7]. This model has been applied to several experimental systems, and, in particular, has been successfully used to explain the parity-breaking bifurcations observed in the directional cooling of nematics [10–12], and in Taylor vortex flow [20]. In the case that the pattern consists of only two modes, the q-$2q$ model reduces to that of Goldstein *et al.* [5], but we were unable to reconcile our results on the printer's instability [28] with the specific predictions of the q-$2q$ model, possibly because our patterns involved many more than just two spatial modes.

Another well-known instability of one-dimensional patterns is the Eckhaus instability [32]. At a supercritical bifurcation to a state with a *stationary* spatial pattern, perturbations of a particular wave number become unstable and grow, while above the onset, a band of wave numbers is linearly unstable. Not all wave numbers within this band lead to stable patterns, however, the stable wave number band of stationary one-dimensional patterns is limited by the Eckhaus instability [32,33]. Patterns with wave numbers lying outside of the Eckhaus boundary are unstable to a long-wavelength phase instability, which eventually leads to the gain or loss of individual pattern units so as to bring the pattern back inside the Eckhaus-stable band. The Eckhaus instability has been studied in several systems displaying stationary patterns [8,34–40]. The Eckhaus instability also affects traveling-wave patterns, but it is only recently that it has been studied in this context [41,42]. Janiaud *et al.* [43,44] have studied the Eckhaus instability in traveling waves produced by the oscillatory instability experimentally in Rayleigh-Bénard convection in compressed argon gas, and analytically and numerically in the framework of the complex Ginzburg-Landau equation. Baxter *et al.* [45], and Kolodner [46,47] have studied the Eckhaus instability in traveling wave convection in binary fluid mixtures. The experiments in each of these cases involved preparing the system in a state outside the Eckhaus-stable band and studying its evolution. A modulation of the pattern's phase develops and grows in amplitude, eventually leading to the gain or loss of one wavelength of the oscillatory pattern in the former case [43], or the creation or annihilation of a pair of convection rolls in the latter case [45–47].

Recently, Cummins *et al.* [26] studied a sequence of bifurcations that occurs in an experimental system similar to ours. They worked in the fourth quadrant of Fig. 1. With v_o fixed at a low (negative) value, v_i was increased. First, the straight interface became unstable to the stationary fingering pattern. Next, a parity-breaking bifurcation to a traveling-finger pattern occurred. At a third transition, the pattern's wavelength suddenly increased by roughly a factor of 2, and the fingers' asymmetry and velocity also increased.

In this paper we report on an experimental study of the broken-parity traveling wave state in the printer's instability, at higher values of the outer cylinder speed than we studied previously [27,28]. In this parameter region, the traveling-finger patterns we observed were never perfectly uniform, and never perfectly stable. Rather, the pattern's local wavelength, and the fingers' asymmetry and traveling speed, varied slowly along the pattern, and the relatively ordered finger patterns were intermittently disrupted by transient bursts of disordered behavior. The variation of wavelength along the pattern allows us to observe what we interpret as the Eckhaus instability for this system: when the local wavelength becomes too long, new fingers are born, while if it is too short, adjacent fingers will merge. A wavelength-changing transition, similar to that observed by Cummins *et al.* [26], was also observed. Despite this fairly complicated dynamical behavior, features of the theory of parity breaking [2,4,5], for example, the connection between traveling speed and asymmetry, remain important.

Our experimental arrangement has been described in detail elsewhere [28]. The apparatus consists of two horizontal, parallel cylinders, mounted acentrically one inside the other. The inner cylinder has radius $r_1 = 50.4$

mm and length $l_1 = 202$ mm, and the transparent outer cylinder has inner radius $r_2 = 66.7$ mm, $l_2 = 210$ mm. The gap between the cylinders is narrowest at the bottom; in these experiments the minimum width of the gap was fixed at 0.5 ± 0.05 mm. Silicone oil with viscosity $\mu = 0.525$ g/cm s, surface tension $\sigma = 19.4$ g/s^2, and density $\rho = 0.963$ g/cm^3 at room temperature, filled the gap [48]. The pattern at the forward oil-air interface was monitored with a CCD video camera and monitor, and data were recorded on a VCR or stored on a personal computer with a frame grabber for later analysis. Finger wavelengths were measured directly from video images. Traveling speeds were determined either by simply measuring the distance a finger moved over a small number of video frames, or from space-time pictures such as Fig. 3 below. The degree of asymmetry of the pattern was determined using a modification of the Fourier transform technique described in Refs. [28,49]. If the interface height, U, is a single-valued function of position, x, we can write it as a Fourier series,

$$U(x) = \sum_{j=1}^{\infty} a_j \cos jqx + \sum_{j=1}^{\infty} b_j \sin jqx, \tag{6}$$

where q is a wave number. We define our origin so that $b_1 = 0$, and then define the asymmetry parameter $\mathcal{A}$ as

$$\mathcal{A} = \left(\frac{\sum b_j^2}{\sum (a_j^2 + b_j^2)} \right)^{1/2}, \tag{7}$$

i.e., as the square root of the fraction of the power contained in the odd terms of the expansion. Over much of the parameter range studied here, the interface height is in fact a multiple-valued function of x, as can be seen in Fig. 2 below. To handle this, we transform the interface pattern to a single valued function $U(l)$, where l is a distance parameter measured along the interface curve itself. We write $U(l)$ as a Fourier series,

$$U(l) = \sum_{j=1}^{\infty} a'_j \cos jq'l + \sum_{j=1}^{\infty} b'_j \sin jq'l, \tag{8}$$

with a new wave number q', and as above we set the coefficient b'_1 equal to zero. We then define a new asymmetry parameter $\mathcal{A}'$ by

$$\mathcal{A}' = \left(\frac{\sum b_j'^2}{\sum (a_j'^2 + b_j'^2)} \right)^{1/2}. \tag{9}$$

By calculating both quantities for a number of single-valued patterns, we can relate $\mathcal{A}'$ to $\mathcal{A}$. In what follows, we present our results in terms of the parameter $\mathcal{A}$, for consistency with our previous work.

The Fourier spectra of the transformed multiple-valued fingers are qualitatively similar to the spectra of similarly transformed single-valued fingers [49]. The amplitude of the second harmonic is typically on the order of 15% of the amplitude of the first, with higher harmonics being weaker. The Fourier spectra of uniform traveling patterns were studied in detail in Ref. [28].

II. RESULTS

Measurements were taken along lines of constant outer cylinder speed, v_o, through the TW state, as indicated in Fig. 1. v_o was fixed at a selected value above the onset of the stationary fingering pattern, and v_i changed in small steps. When v_o is small, i.e., close to the onset of the stationary pattern, a spatially uniform traveling-wave pattern of fingers develops via a supercritical parity-breaking transition. The behavior of the pattern in this region has been reported elsewhere [27,28], and is in accord with what is expected from the theory of Coullet *et al.* [2,5]. The phase speed v_ϕ is linear in the asymmetry of the pattern and proportional to the square root of $v_i - v_i^*$, where v_i^* is the value of v_i at the parity-breaking transition, over the entire range of existence of the traveling-wave state.

At higher values of v_o, however, the behavior of the traveling-wave patterns is more complex, and it is this region with which we are concerned here. Figure 2 shows a series of finger patterns observed for $v_o = 174$ mm/s, as v_i is increased. The stationary pattern is unstable at the lowest values of v_i we can study, and is replaced by a disordered state consisting of regions of traveling fingers, whose speed and amplitude are time dependent, separated by source and sink defects. At lower values of v_o, this disordered state eventually relaxed to a uniform traveling pattern [27,28]. However, at the outer cylinder speeds studied here, at low v_i, the disordered state never settles down, consistent with the theoretical prediction that the uniform traveling-wave state is unstable at onset [7].

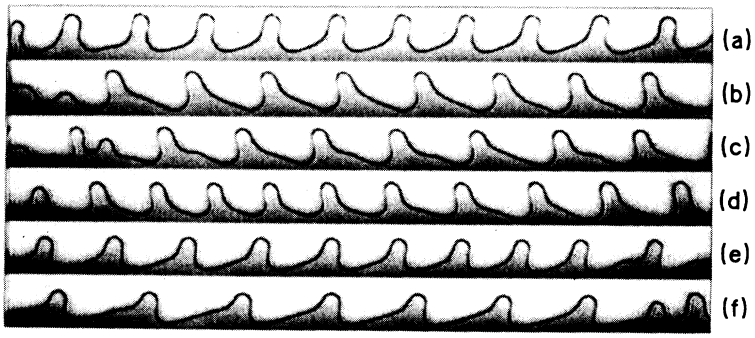

FIG. 2. Traveling-finger patterns at $v_o = 174.3$ mm/s. (a) $v_i = 6.33$ mm/s; (b) $v_i = 12.67$ mm/s; (c) $v_i = 15.83$ mm/s; (d) $v_i = 17.42$ mm/s; (e) $v_i = 23.75$ mm/s; (f) $v_i = 33.25$ mm/s. The images show 174 mm of the pattern's length.

As v_i is increased, a more ordered traveling-wave state eventually appears, as shown in Fig. 2(a). This pattern is never perfectly uniform, however, nor is it stable in time. Source or sink defects can remain in the pattern, typically near the end of the apparatus, but usually the traveling fingers appear at one end of the apparatus and disappear at the other. At any given time, the wavelength of the pattern changes along its length. In Fig. 2(a) this variation is about 5%; it is more obvious in Fig. 2(d), where the wavelength increases by about 25% from left to right. When the fingers are moving away from a source defect, the pattern's wavelength increases along its direction of propagation, while if they are moving towards a sink defect, the wavelength decreases. Furthermore, this pattern only exists for, typically, a few minutes at a time, after which it again becomes disordered. After a few seconds, the disorder passes and the pattern returns to one like that of Fig. 2(a), and so on. Patterns moving in either direction (and thus with either sense of asymmetry) can occur, and often the direction of propagation is reversed after the passage of a disorded burst.

As v_i is further increased, the pattern's average wavelength, phase speed, and finger asymmetry all increase, as was found for the uniform traveling patterns at lower v_o. The variation in wavelength along the pattern also becomes more pronounced, and the intermittent bursts of disorder more frequent. Patterns from this regime are illustrated in Figs. 2(b) and 2(c). A sudden transition occurs between Figs. 2(c) and 2(d), at which the pattern's average wavelength drops, and the phase speed and asymmetry of the fingers also decrease. As v_i is increased above this transition, the wavelength of the traveling pattern becomes more uniform and the frequency of the disordered periods decreases, and the average wavelength, speed, and asymmetry increase again, as shown in Figs. 2(e) and 2(f). Eventually, the SW region of Fig. 1 is reached, in which localized patches of broken parity symmetry travel through a background pattern of stationary fingers, then the stationary finger state, and, finally, the straight interface reappears.

Figure 3 is a space-time image, showing the motion of a pattern traveling to the left over a period of 24 seconds. For this pattern, $v_o = 174$ mm/s and $v_i = 23.8$ mm/s, as in Fig. 2(e). This picture illustrates the increase in the wavelength and traveling speed of the fingers in the pattern as they move along the length of the apparatus.

The way in which the pattern's characteristics vary along the interface, at a fixed time, is illustrated in Fig. 4. The particular image from which the data were taken is shown in Fig. 4(a) (note that the interface extends roughly one wavelength further than shown on both the right and left ends of the figure). The fingers propagate away from the source defect at the left side of the image, so most of the pattern is moving to the right. The local wavelength, defined as the distance between adjacent minima in the interface height, the asymmetry of each individual finger, and each finger's traveling speed are shown as a function of position, in Figs. 4(b)–4(d). In the case of fingers propagating away from a source closer to the middle of the apparatus, the properties of the pattern on the two sides of the defect have inversion symmetry, as expected. The finger closest to the source in Fig. 4(a) is longer, more asymmetric and faster moving than its neighbors. This reflects the mechanism by which new fingers appear at the source. Existing fingers move away from the defect. When the distance between the source and the nearest finger becomes too large, a small ripple appears close to the defect, which is reabsorbed if it is too close to the defect's core; otherwise, it propagates away as a new finger. New fingers initially move quickly, but slow down when they have caught up with the rest of the drifting pattern. Near a sink defect, the opposite behavior is observed: the pattern slows and becomes compressed, until a finger disappears into the sink. This behavior is similar to that observed at the Eckhaus instabilty of the pattern, which we discuss below.

Once far enough (i.e., a few wavelengths) away from the source, the pattern's wavelength, speed and asymmetry all increase in a similar way, and appear to be saturating towards the end of the apparatus. Figure 5(a)

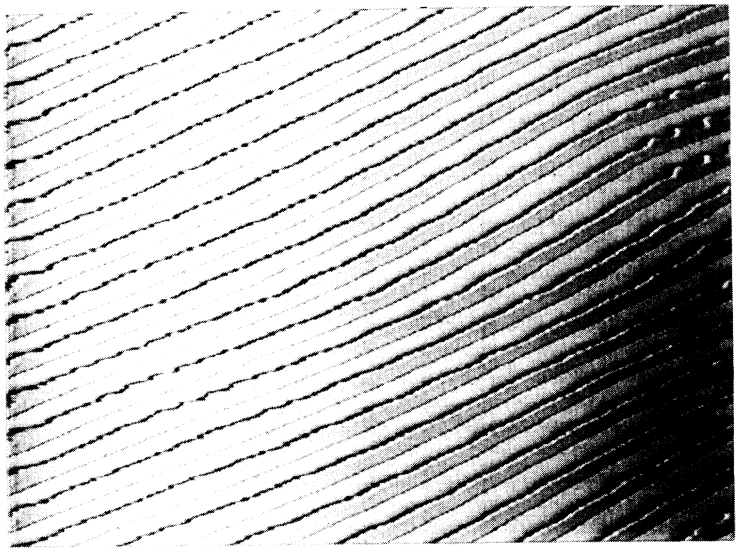

FIG. 3. A space-time image of a pattern traveling to the left at $v_o = 174.3$ mm/s, $v_i = 23.75$ mm/s. The speed and wavelength of the fingers increase as they move along the length of the apparatus. Time runs from top to bottom and the figure covers 24 s. 151 mm of the pattern are shown.

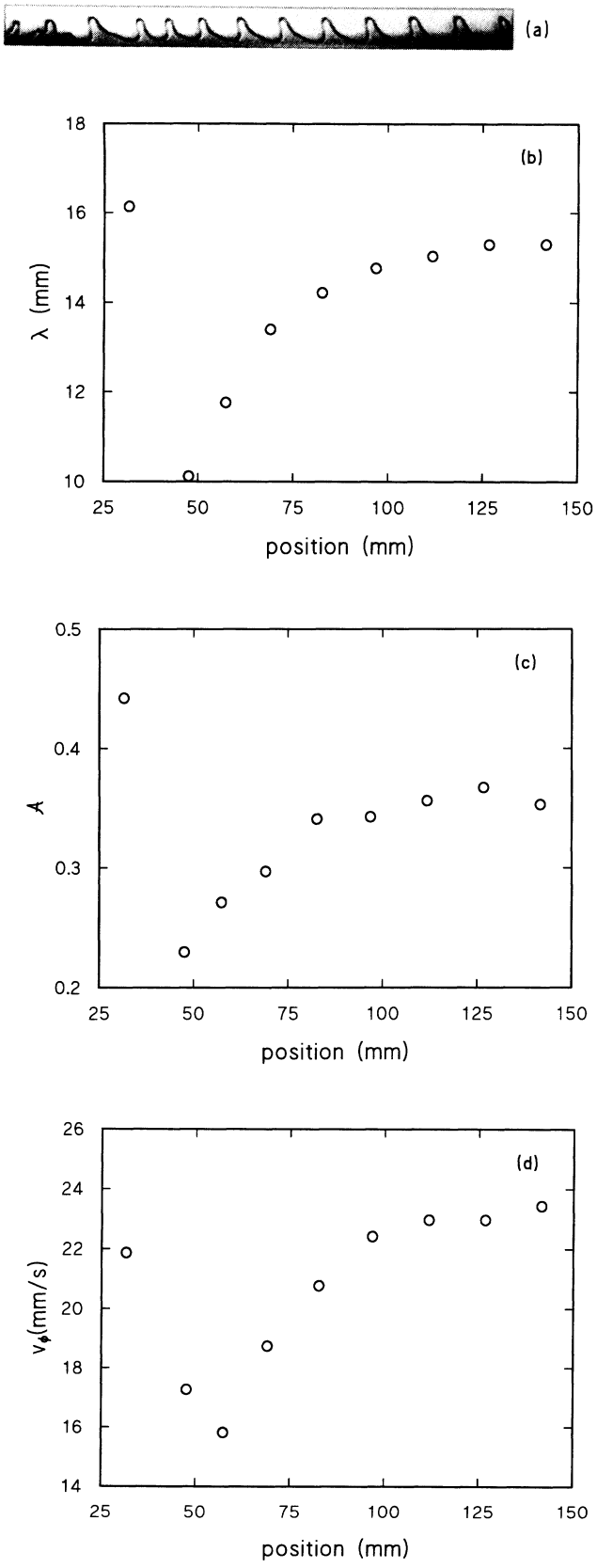

FIG. 4. The variation of the local properties of a nonuniform traveling pattern, as a function of position, for v_o = 261.4 mm/s, v_i = 55.42 mm/s. (a) The pattern itself. (b) The local wavelength, λ. (c) The asymmetry of the fingers, $\mathcal{A}$. (d) The local traveling speed, v_ϕ.

is a plot of phase speed vs asymmetry for the individual fingers in this pattern, as well as for fingers from patterns at two other values of the cylinder speeds. The fingers in the pattern display a linear dependence of phase speed on asymmetry, as did the uniform traveling-finger patterns studied previously [27,28]. Straight-line fits to these data sets have intercepts equal to zero within error, indicating that, even for these patterns where the wavelength is not constant, the ϕ_{xx} term in Eq. (3) is small. The slope of the v_ϕ vs $\mathcal{A}$ graph is the parameter ω of Eq. (3). ω is plotted as a function of v_o in Fig. 5(b), which includes a data point for the uniform traveling-finger states of Ref. [28]. Figure 5(b) indicates that ω is proportional to $v_o - v_{oc}$, where v_{oc} is the value of v_o at which the stationary finger pattern appears when $v_i = 0$. A fit to the data, shown in the figure as a dashed line, gives $\omega = 0.40 \pm 0.02(v_o - v_{oc})$.

Figure 6(a) is a plot of the square of the pattern's average phase speed against the control parameter, v_i, and Fig. 6(b) shows the square of the asymmetry parameter $\mathcal{A}$ as a function of v_i. v_ϕ^2 is linear in v_i at low v_i, in agreement with our results for the spatially uniform traveling patterns [27,28]; here the bifurcation to the broken-parity state occurs at $v_i = 0$ within our experimental resolution. At $v_i \approx 16$ mm/s, the wavelength-changing transition described above occurs and the phase speed suddenly drops. As shown in Fig. 6(b), a drop in the average asymmetry of the fingers occurs simultaneously. In a plot of v_ϕ vs $\mathcal{A}$, however, there is no sign of this transition: data from above and below the transition fall on the same continuous curve, as shown in Fig. 7. The relationship between v_ϕ and the asymmetry parameter is linear at low values of $\mathcal{A}$, as found for the spatially uniform patterns [27,28], but, in contrast to what was found in that case, the linearity no longer persists over the whole range of existence of the traveling state.

The pattern's behavior changes as the rotation speed of the outer cylinder is increased. The range of existence of the disordered state at low v_i increases, and the wavelength-changing transition moves to higher values of v_i. The transition also becomes weaker, i.e., the magnitudes of the changes in average phase velocity, wavelength, and asymmetry all become smaller. At relatively high values of v_o, the transition disappears completely. At these high values of v_o, the transient bursts of disorder seen at lower v_o no longer occur. Figure 8 is a plot of v_ϕ^2 vs v_i for v_o = 436 mm/s; the square of the phase speed increases linearly with v_i at low v_i, then smoothly decreases as the transition back to stationary fingers is approached. At this value of v_o, no sudden drop in v_ϕ is visible in the traveling-wave state.

The variation of wavelength along the patterns leads to the creation or annihilation of fingers via what appears to be an Eckhaus instability. As the fingers move away from a source, their wavelength grows. When the local wavelength becomes larger than a certain value, the finger becomes unstable and ripples start to appear on the forward side (i.e., the less steeply sloped side) of the finger's base. Some of these can be seen in Fig. 2, for example, at the right-hand side of Fig. 2(e). These ripples represent attempts at the formation of new fingers. Sometimes these attempts are unsuccessful: the ripple moves back

towards, and is reabsorbed by, the parent finger. If the ripple initially develops far enough from the parent finger, however, it will grow and move away, forming a new, independent finger, and causing the local wavelength to decrease back into the stable range. New fingers develop at source defects in a similar way, as described above.

This process is illustrated in Figs. 9 and 10. Figure 9 is a sequence of images of the interface for $v_o = 240$ mm/s and $v_i = 47.5$ mm/s. The pattern in this case is moving to the left. Initially [Fig. 9(a)], the fingers at the left-hand side of the front have a wavelength which is too long, and they are unstable. A new finger is trying to nucleate just in front of the finger labeled 1 in Fig. 9(a), but it is too close, and in Fig. 9(b) it is in the process of being reabsorbed by finger 1. Another attempt is made in Fig. 9(c), with the same result: the new finger is reabsorbed in Fig. 9(d). In Fig. 9(d), the finger labeled 2 has also become unstable, and a small ripple can be seen developing in front of that finger. Again the new finger is reabsorbed, as shown in Figs. 9(e) and 9(f). Finally, in Fig. 9(g), a new finger successfully forms; it can be seen moving away from its parent finger in Figs. 9(h)–9(j). The time elapsed from the start to the end of Fig. 9 is 2.73 s.

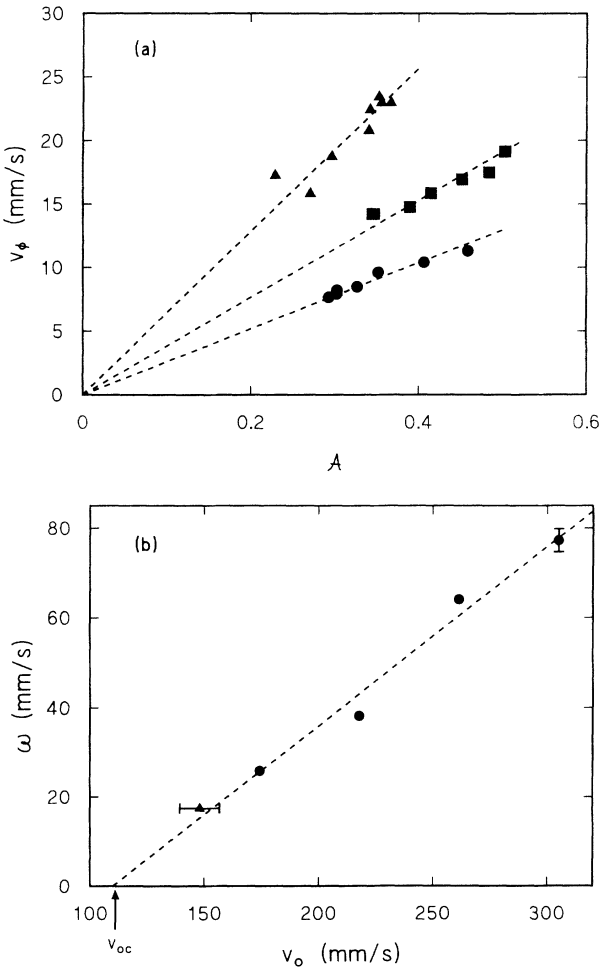

FIG. 5. (a) The phase speed plotted against asymmetry for each finger in three nonuniform patterns at different cylinder speeds. Circles: $v_o = 174.3$ mm/s, $v_i = 23.75$ mm/s; squares: $v_o = 217.8$ mm/s, $v_i = 55.42$ mm/s; triangles: $v_o = 261.4$ mm/s, $v_i = 55.42$ mm/s. The data shown as triangles are from the pattern of Fig. 4. The slopes of the lines through the data give the parameter ω of Eq. (3). (b) ω as a function of v_o. The circles are from the present work, and the triangle from our study of the uniform traveling wave states in Refs. [27,28]. The arrow indicates v_{oc}, the onset value for the stationary fingering pattern.

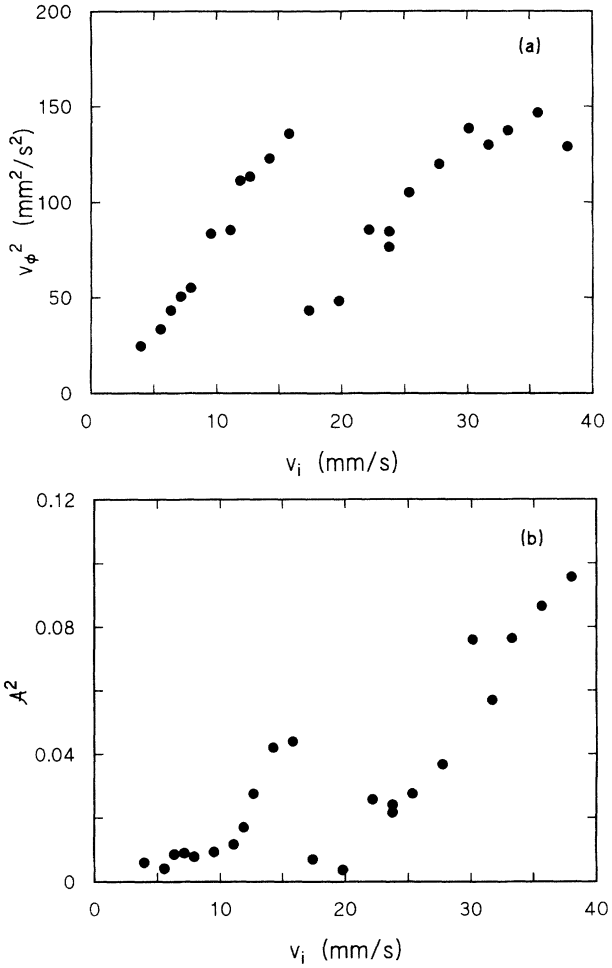

FIG. 6. (a) v_ϕ^2 and (b) $\mathcal{A}^2$ plotted against v_i, for $v_o = 174.3$ mm/s.

Figure 10 is a space-time representation of a similar sequence of events at $v_o = 174$ mm/s, $v_i = 22.2$ mm/s. The time from top to bottom of the figure is 13.5 s. As in the case discussed above, prior to the creation of the new finger, there are several unsuccessful attempts, both on the eventual parent finger and its neighbors. These show up on the space-time picture as modulations in the widths of the fingers.

Observations of events such as these allow us to construct a stability diagram for broken-parity traveling waves in this system. We take the long-wavelength stability limit of the fingers to be defined by the wavelength at which the ripples, which represent attempts to create new fingers, first appear. The short-wavelength limit is given by the smallest interfinger spacing for which the

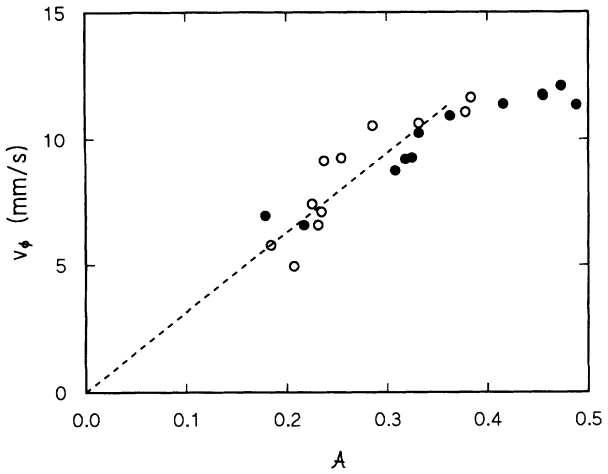

FIG. 7. Traveling speed, v_ϕ, as a function of asymmetry for the data of Fig. 6. The open and solid symbols indicate data from below and above the transition at $v_i \approx 16$ mm/s, respectively.

two fingers do not recombine. The results of these measurements are shown in a plot of control parameter, v_i, against wavelength for two values of v_o in Fig. 11. The data points at $v_i = 0$ indicate the wavelength of the stationary pattern there. Between $v_i = 0$ and the lowest-v_i data points in the figure, the pattern was disordered and measurements of the stability boundary were not possible. The data for $v_o = 218$ mm/s (the circles) show a definite kink, most obvious on the high-wavelength side of the stability boundary. This kink coincides with the transition discussed above, at which the pattern's wavelength suddenly changes. The kink does not appear in data taken at high values of v_o (for example, the stars in Fig. 11), for which the transition does not occur. While the low-wavelength side of the boundary doesn't change much as v_o is varied, the high-wavelength side moves in and the stable region becomes more narrow as v_o is increased. The propagating finger pattern normally appears to select wavelengths near the long-wavelength stability boundary, and fingers with shorter wavelengths are only seen during creation or annihilation events.

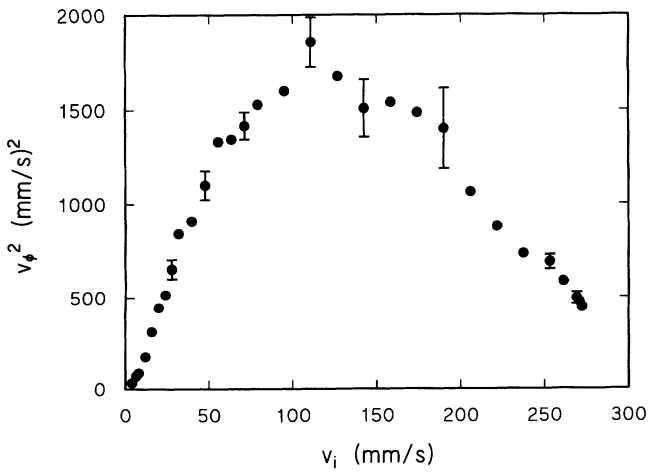

FIG. 8. v_ϕ^2 as a function of v_i at $v_o = 435.7$ mm/s.

III. DISCUSSION

At very small values of v_i, the patterns we observe are spatially and temporally disordered, as described above, and at higher v_i, the disorder persists in the form of intermittent disruptions of the nonuniform broken-parity state. In our measurements at lower v_o [27,28], and in Ref. [26], the disordered state was transient. A spatially-uniform broken-parity state is expected, on the basis of a stability analysis of a generalized version of Eqs. (2) and (3), to be unstable at onset [7]. In the Appendix, we show that spatially-uniform solutions of Eqs. (2) and (3) themselves, without any additional terms, are also linearly unstable to long-wavelength perturbations close to onset. The nonuniformity of the patterns we have studied here may be a manifestation of this instability. Indeed, given that the uniform traveling-wave state is unstable at onset, the nonuniformity of the traveling-wave states studied in this work is perhaps less surprising than the fact that the disordered state eventually gives way to a stable, uniform state at low values of v_o in Refs. [27,28], and also in Ref. [26]. The uniformity in those cases may be a result of the finite length of the experimental apparatus [30], or a nonlinear effect not accounted for in the linear stability analysis. The temporal coexistence of the disordered state with the nonuniform traveling patterns reported above is also interesting. The intermittent appearances of the disordered pattern are related to the wavelength-changing transition we observe—the disorder apperars more frequently near the transition—but the nature of the relationship is not understood.

In Ref. [26], Cummins *et al.* describe a series of transitions in fingering patterns in an experiment very similar to the one discussed here. Although they worked in a different parameter range, there is substantial agreement between their results and ours. Cummins *et al.* did some experiments with v_i fixed at a value well above the onset of stationary fingers, and varied v_o, following vertical lines downward in the fourth quadrant of Fig. 1. Cummins *et al.* observed that, as v_o is decreased below zero, the pattern is initially disordered, as in our case, but that after roughly ten minutes, it settles down to a uniform traveling wave, possibly with defects. In our case, transient disordered states continue to reappear every few minutes. As they moved further down in v_o, their pattern wavelength increased, and then, at a discontinuous transition, it suddenly decreased. This behavior is analogous to what we observe in the second quadrant of Fig. 1.

In another set of experiments reported in Ref. [26], Cummins *et al.* fixed v_o at a small negative value, then increased v_i along horizontal lines in the fourth quadrant of Fig. 1. Beyond the parity-breaking transition, the wavelength of their pattern decreased. They then saw a transition at which the wavelength suddenly increased by roughly a factor of 2, before decreasing again as v_i was further raised. The phase diagram they construct on the basis of their observations is consistent with what we observe.

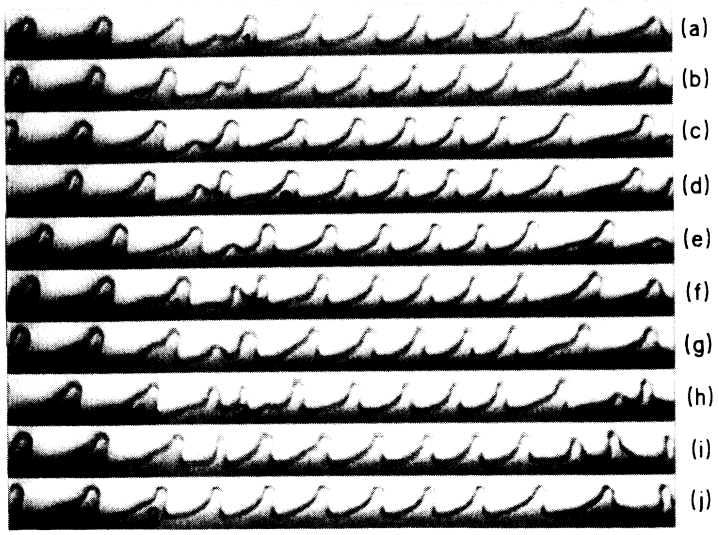

FIG. 9. The formation of a new finger when the local wavelength becomes too long. Here $v_o = 239.6$ mm/s and $v_i = 47.50$ mm/s. The images were recorded at times (a) 0 s; (b) 0.10 s; (c) 0.23 s; (d) 0.35 s; (e) 0.68 s; (f) 0.83 s; (g) 1.00 s; (h) 1.23 s; (i) 1.73 s; and (j) 2.73 s.

Cummins *et al.* [26] also note that the short-wavelength fingers they observe before the wavelength-changing transition had well-defined wavelengths, but some scatter in velocity. In contrast, the long wavelength fingers observed above the transition had considerable scatter in their wavelength, but well defined velocities. We observe a systematic variation in both wavelength and velocity with position in the pattern, rather than random scatter, and, as shown in Fig. 4, the variations are coupled. An important point is that for the long-wavelength fingers in Ref. [26] as well as for our patterns, the wavelength selection is not perfect, and in both cases a range of wavelengths is observed.

Despite their nonuniformity, and their intermittent disruption by the disordered bursts, aspects of the behavior derived in the context of spatially-uniform broken-parity waves remain valid for our patterns. At low v_i, the pattern's average phase speed, v_ϕ, grows as the square root of v_i, as shown in Fig. 6(a). While our data for the asymmetry, $\mathcal{A}$, are noisier, it appears that the average of $\mathcal{A}$ is also proportional to $v_i^{1/2}$ at low v_i. Figure 7 shows that v_ϕ is proportional to $\mathcal{A}$ at low speeds. The linear relationship between v_ϕ and $\mathcal{A}$ also holds for the individual fingers in the pattern at a given time, as was illustrated in Fig. 4. These results are all in agreement with the theoretical [2,5] and experimental [27,28] results for uniform patterns.

Goldstein *et al.* [4,5] have discussed the behavior of broken-parity traveling waves near spatiotemporal defects. They studied a generalization of the coupled equations, Eqs. (2) and (3), in which ϕ is the phase of a complex field, and observe that the mechanism by which fingers vanish at a sink defect in their model is very similar to that of the Eckhaus instability. In Fig. 14 of Ref. [5], they show patterns near source and sink defects, calculated from their model. At the defect, the broken-parity order parameter approaches zero, which causes distortions of the pattern. Close to a sink, the pattern is compressed and its phase speed smaller relative to the uniform, propagating pattern far from the defect. Near a source, the pattern is stretched and travels faster. This behavior is in accord with what we observe close to source

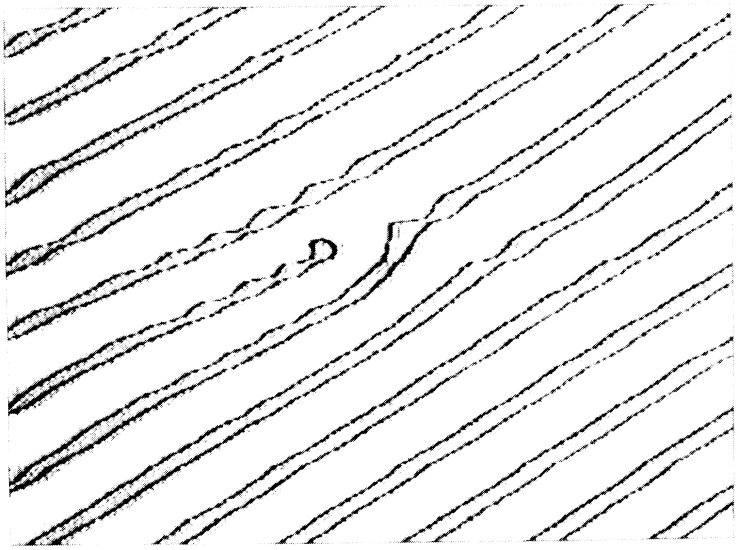

FIG. 10. A space-time image of a drifting pattern showing the nucleation of a new finger. Here $v_o = 174$ mm/s, $v_i = 22.2$ mm/s. Time runs from the top down, and the total time is 13.5 s; 91.6 mm of the system length is shown.

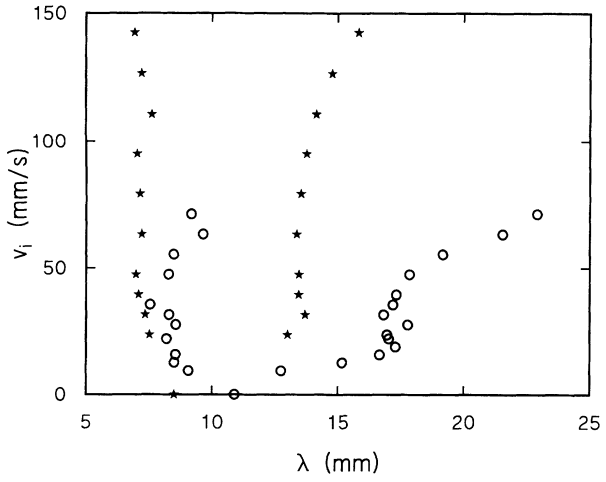

FIG. 11. The measured Eckhaus stability boundary for traveling waves in our experiment, for two values of v_o. Outside of the boundary the fingers become unstable, resulting in the creation of a new finger on the long-wavelength side, or in the loss of a finger on the short-wavelength side. Circles: $v_o = 217.9$ mm/s; stars: $v_o = 348.6$ mm/s.

and sink defects, as described above, although our patterns are not uniform away from the defects in this parameter range.

As mentioned in Sec. I, previous measurements of the Eckhaus instability in traveling-wave systems were done by manipulating the system so as to attain a state with an average wavelength outside of the Eckhaus-stable band [43,45–47]. The evolution of the pattern was then studied. The Eckhaus instability is a phase instability, and, at least initially, manifests itself as a spatial modulation of the pattern's local wave number, with the pattern amplitude remaining constant. As the instability develops, amplitude variations eventually appear, and, at the point in space time at which the pattern gains or loses a pattern unit, the amplitude must go to zero.

The situation in our experiment is rather different. Here, we do not prepare the system in any particular initial state. Rather, the system selects a spatially nonuniform state of its own accord, and the dynamics of this state lead to the occurrence of an instability when the pattern's wavelength evolves out of a stable wavelength band. This instability results in the birth or death of fingers, so as to bring the wavelength back inside the stable band. This adjustment of wave number by the creation or annihilation of pattern units is characteristic of the Eckhaus instability. We have assumed that the wavelength at which new fingers first attempt to develop corresponds to the long-wavelength boundary of the Eckhaus-stable wavelength band, and that the minimum wavelength below which adjacent fingers merge corresponds to the short-wavelength boundary. However, the nonuniformity of the wavelength along our patterns suggests that the pattern is already subject to a phase instability, independent of the creation or annihilation of fingers. We suggested above that this nonuniformity was related to the instability of the broken-parity wave at its onset.

IV. SUMMARY

We have presented experimental results on the dynamics of broken-parity traveling-finger patterns in the printer's instability. In the range of control parameters we studied here, the phenomenology of our system is quite complex. The pattern is unstable at the onset of parity-breaking, as predicted theoretically [7], and the instability persists above onset in the form of spatial nonuniformities of the pattern, and intermittent bursts of disorder which disrupt the pattern. The pattern is also subject to the Eckhaus instability, which limits the band of wave numbers over which the individual traveling fingers are stable. In spite of this complexity, some basic results of the theory of parity breaking in patterns [5], in particular the relationship between the pattern's asymmetry and its traveling speed, remain valid. There are several of our results which warrant further investigation, including the nature of the transient disordered bursts and their connection with the wavelength-changing transition discussed above, and a complete understanding of this system will also require further theoretical study.

ACKNOWLEDGMENT

This research was supported by the Natural Sciences and Engineering Research Council of Canada.

APPENDIX: LINEAR STABILITY ANALYSIS OF SPATIALLY-UNIFORM BROKEN-PARITY WAVES

We consider Eqs. (2) and (3), which we repeat here for convenience:

$$A_t = A_{xx} + \mu A - A^3 + \epsilon \phi_x A \,, \tag{A1}$$

$$\phi_t = \phi_{xx} + \omega A. \tag{A2}$$

A is the amplitude and ϕ the relative phase of a propagating broken-parity wave. μ is the control parameter, and ϵ and ω are constants. These equations have a spatially-uniform solution given by $A = A_0$, $\phi_{0x} = [(q - q_0)/q_0]$, where q_0, the wave number of the underlying, symmetric pattern, and q, the wave number of the pattern with broken parity, are independent of x.

Inserting these solutions into Eqs. (A1) and (A2), it is straightforward to show that, in a steady state,

$$A_0 = [\mu + \epsilon(q - q_0)/q_0]^{1/2} \tag{A3}$$

and

$$\phi_{0t} = \omega A_0. \tag{A4}$$

Since A_0 is real, this solution exists for

$$A_0^2 = \mu + \epsilon(q - q_0)/q_0 > 0, \tag{A5}$$

as shown in Fig. 12. We now add a small perturbation A_0 to test the stability of the uniform solution. We write

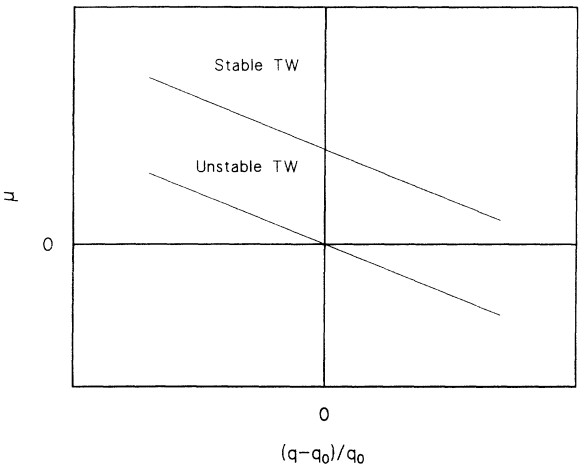

FIG. 12. Linear stability diagram of the spatially-uniform traveling-wave state.

$$A = A_0 + A_1 e^{ikx+\lambda t}, \tag{A6}$$

$$\phi = \phi_0 + \phi_1 e^{ikx+\lambda t}, \tag{A7}$$

where k is the wave number of the perturbation and λ its growth rate; for the unperturbed solution to be stable we must have $\mathrm{Re}\{\lambda\} < 0$. Substituting Eqs. (A6) and (A7) into Eqs. (A1) and (A2), and linearizing in the small perturbations, we get

$$\left(\lambda + k^2 + 2A_0^2\right) A_1 - i\epsilon k A_0 \phi_1 = 0, \tag{A8}$$

$$\omega A_1 - \left(\lambda + k^2\right) \phi_1 = 0. \tag{A9}$$

The characteristic equation for λ is

$$\lambda^2 + \lambda\beta + \gamma = 0, \tag{A10}$$

with

$$\beta = 2(k^2 + A_0^2) \tag{A11}$$

and

$$\gamma = k^2(2A_0^2 + k^2) - i\omega\epsilon k A_0. \tag{A12}$$

In the long-wavelength limit, i.e., $k \to 0$, $\gamma \ll \beta^2$, so, to order k^4, the solutions for λ are

$$\lambda = -\frac{\beta}{2} \pm \left(\frac{\beta}{2} - \frac{\gamma}{\beta} - \frac{\gamma^2}{\beta^3}\right). \tag{A13}$$

Taking the largest of the two solutions to Eq. (A13), the stability requirement becomes

$$\mathrm{Re}\left\{\frac{\gamma}{\beta} + \frac{\gamma^2}{\beta^3}\right\} > 0, \tag{A14}$$

from which, using the definitions of γ and β, we find that the uniform solution is stable for

$$A_0^2 = \mu + \epsilon\left(\frac{q - q_0}{q_0}\right) > \frac{|\epsilon\omega|}{2\sqrt{2}}. \tag{A15}$$

Thus, spatially uniform solutions exist, but are unstable, in the range

$$0 < \mu + \epsilon\left(\frac{q - q_0}{q_0}\right) < \frac{|\epsilon\omega|}{2\sqrt{2}}, \tag{A16}$$

as shown in Fig. 12. The coupling terms in Eqs. (A1) and (A2) are always destabilizing, regardless of the sign of the coupling constants ω and ϵ. This result agrees with that of Fauve *et al.* [7], derived from a more general version of the equations of motion.

[1] M.C. Cross and P.C. Hohenberg, Rev. Mod. Phys. **65**, 851 (1993).
[2] P. Coullet, R.E. Goldstein, and G.H. Gunaratne, Phys. Rev. Lett. **63**, 1954 (1989).
[3] P. Coullet and G. Iooss, Phys. Rev. Lett. **64**, 866 (1990).
[4] R.E. Goldstein, G.H. Gunaratne, and L. Gil, Phys. Rev. A **41**, 5731 (1990).
[5] R.E. Goldstein, G.H. Gunaratne, L. Gil, and P. Coullet, Phys. Rev. A **43**, 6700 (1991).
[6] S. Fauve, S. Douady, and O. Thual, Phys. Rev. Lett. **65**, 385 (1990).
[7] S. Fauve, S. Douady, and O. Thual, J. Phys. (Paris) II **1**, 311 (1991).
[8] A.J. Simon, J. Bechhofer, and A. Libchaber, Phys. Rev. Lett. **61**, 2574 (1988).
[9] J.-M. Flesselles, A.J. Simon, and A.J. Libchaber, Adv. Phys. **40**, 1 (1991).
[10] H. Levine and W.-J. Rappel, Phys. Rev. A **42**, 7475 (1991).
[11] H. Levine, W.-J. Rappel, and H. Riecke, Phys. Rev. A **43**, 1122 (1991).
[12] W.-J. Rappel and H. Riecke, Phys. Rev. A **45**, 846 (1992).
[13] G. Faivre, S. de Cheveigne, C. Guthmann, and P. Kurowski, Europhys. Lett. **9**, 779 (1989).
[14] G. Faivre and J. Mergy, Phys. Rev. A **45**, 7320 (1992).
[15] G. Faivre and J. Mergy, Phys. Rev. A **46**, 963 (1992).
[16] K. Kassner and C. Misbah, Phys. Rev. Lett. **65**, 1458 (1990).
[17] B. Caroli, C. Caroli, and S. Fauve, J. Phys. (Paris) I **2**, 281 (1992).
[18] K. Kassner, A. Valance, C. Misbah, and D. Temkin, Phys. Rev. E **48**, 1091 (1993).
[19] J.T. Gleeson, P.L. Finn, and P.E. Cladis, Phys. Rev. Lett. **66**, 236 (1991).
[20] H. Riecke and H.-G. Paap, Phys. Rev. A **45**, 8605 (1992).
[21] R. Wiener and D.F. McAlister, Phys. Rev. Lett. **69**, 2915 (1992).
[22] I. Mutabazi and C.D. Andereck, Phys. Rev. Lett. **70**, 1429 (1993).
[23] M. Rabaud, S. Michalland, and Y. Couder, Phys. Rev. Lett. **64**, 184 (1990).

[24] Y. Couder, S. Michalland, M. Rabaud, and H. Thomé, in *Nonlinear Evolution of Spatio-Temporal Structures in Dissipative Continuous Systems*, edited by F.H. Busse and L. Kramer (Plenum, New York, 1990), p. 487.
[25] M. Rabaud, Y. Couder, and S. Michalland, Eur. J. Mech., B/Fluids **10**, 253 (1991).
[26] H.Z. Cummins, L. Fortune, and M. Rabaud, Phys. Rev. E **47**, 1727 (1993).
[27] L. Pan and J.R. de Bruyn, Phys. Rev. Lett. **70**, 1791 (1993).
[28] L. Pan and J.R. de Bruyn, Phys. Rev. E **49**, 483 (1994).
[29] V. Hakim, M. Rabaud, H. Thomé, and Y. Couder, in *New Trends in Nonlinear Dynamics and Pattern-Forming Phenomena,* edited by P. Coullet and P. Huerre (Plenum, New York, 1990), p. 327.
[30] L. Pan and J.R. de Bruyn (unpublished).
[31] S. Michalland, M. Rabaud, and Y. Couder, Europhys. Lett. **22**, 17 (1993).
[32] W. Eckhaus, *Studies in Nonlinear Stability* (Springer, Berlin, 1965).
[33] L. Kramer and W. Zimmermann, Physica D **16**, 221 (1985).
[34] M. Boucif, J.E. Wesfreid, and E. Guyon, J. Phys. (Paris) Lett. **45**, L413 (1984).
[35] M. Lowe and J.P. Gollub, Phys. Rev. Lett. **55**, 2575 (1986).
[36] M.A. Dominguez-Lerma, D.S. Cannell, and G. Ahlers, Phys. Rev. A **34**, 4956 (1986).
[37] G. Ahlers, D.S. Cannell, M.A. Dominguez-Lerma, and R. Heinrichs, Physica D **23**, 202 (1986).
[38] H. Riecke and H.-G. Paap, Phys. Rev. A **33**, 547 (1986).
[39] S. Rasenat, E. Braun, and V. Steinberg, Phys. Rev. A **43**, 5728 (1991).
[40] L. Fortune, W.-J. Rappel, and M. Rabaud (unpublished).
[41] W. van Saarloos and P.C. Hohenberg, Physica D **56**, 303 (1992).
[42] H.R. Brand and R.J. Deissler, Phys. Rev. A **45**, 3732 (1992).
[43] B. Janiaud, A. Pumir, D. Bensimon, V. Croquette, H. Richter, and L. Kramer, Physica D **55**, 269 (1992).
[44] B. Janiaud, E. Guyon, D. Bensimon, and V. Croquette, in *Nonlinear Evolution of Spatio-Temporal Structures in Dissipative Continuous Systems,* edited by F.H. Busse and L. Kramer, NATO Advanced Study Institute Ser. B2, Vol. 225 (Plenum, New York, 1990), p. 45.
[45] G.W. Baxter, K.D. Eaton, and C.M. Surko, Phys. Rev. A **46**, 1735 (1992).
[46] P. Kolodner, Phys. Rev. A **46**, 1739 (1992).
[47] P. Kolodner, Phys. Rev. A **46**, 6431 (1992).
[48] Aldrich Chemical Corp., Catalog No. 14,615-3.
[49] L. Pan and J.R. de Bruyn, in *Spatio-Temporal Patterns in Nonequilibrium Complex Systems*, edited by P. Caldis and P. Palffy-Muhoray (Addison-Wesley, Redwood City, CA, in press).

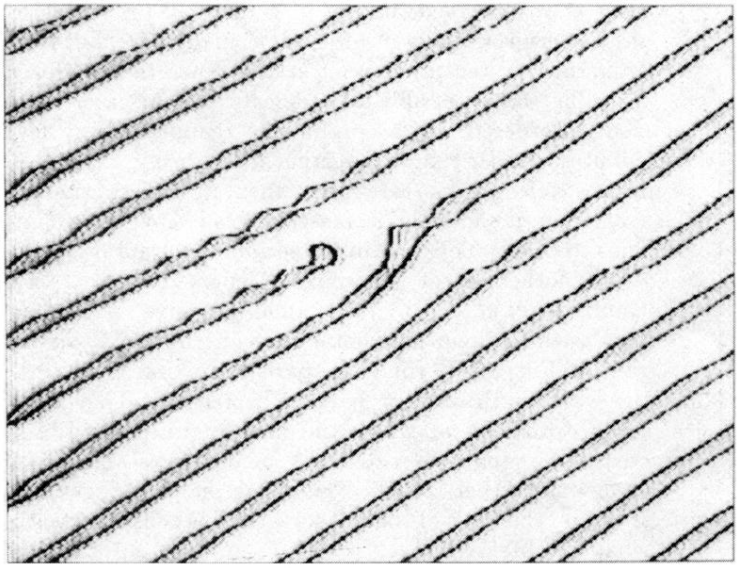

FIG. 10. A space-time image of a drifting pattern showing the nucleation of a new finger. Here $v_o = 174$ mm/s, $v_i = 22.2$ mm/s. Time runs from the top down, and the total time is 13.5 s; 91.6 mm of the system length is shown.

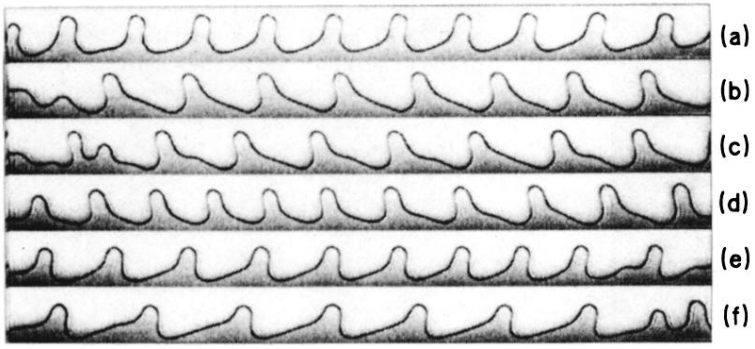

FIG. 2. Traveling-finger patterns at $v_o = 174.3$ mm/s. (a) $v_i = 6.33$ mm/s; (b) $v_i = 12.67$ mm/s; (c) $v_i = 15.83$ mm/s; (d) $v_i = 17.42$ mm/s; (e) $v_i = 23.75$ mm/s; (f) $v_i = 33.25$ mm/s. The images show 174 mm of the pattern's length.

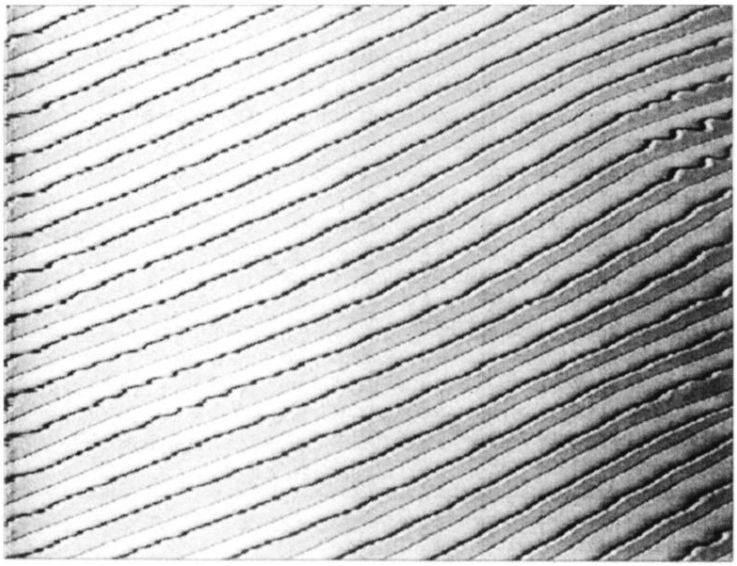

FIG. 3. A space-time image of a pattern traveling to the left at $v_o = 174.3$ mm/s, $v_i = 23.75$ mm/s. The speed and wavelength of the fingers increase as they move along the length of the apparatus. Time runs from top to bottom and the figure covers 24 s. 151 mm of the pattern are shown.

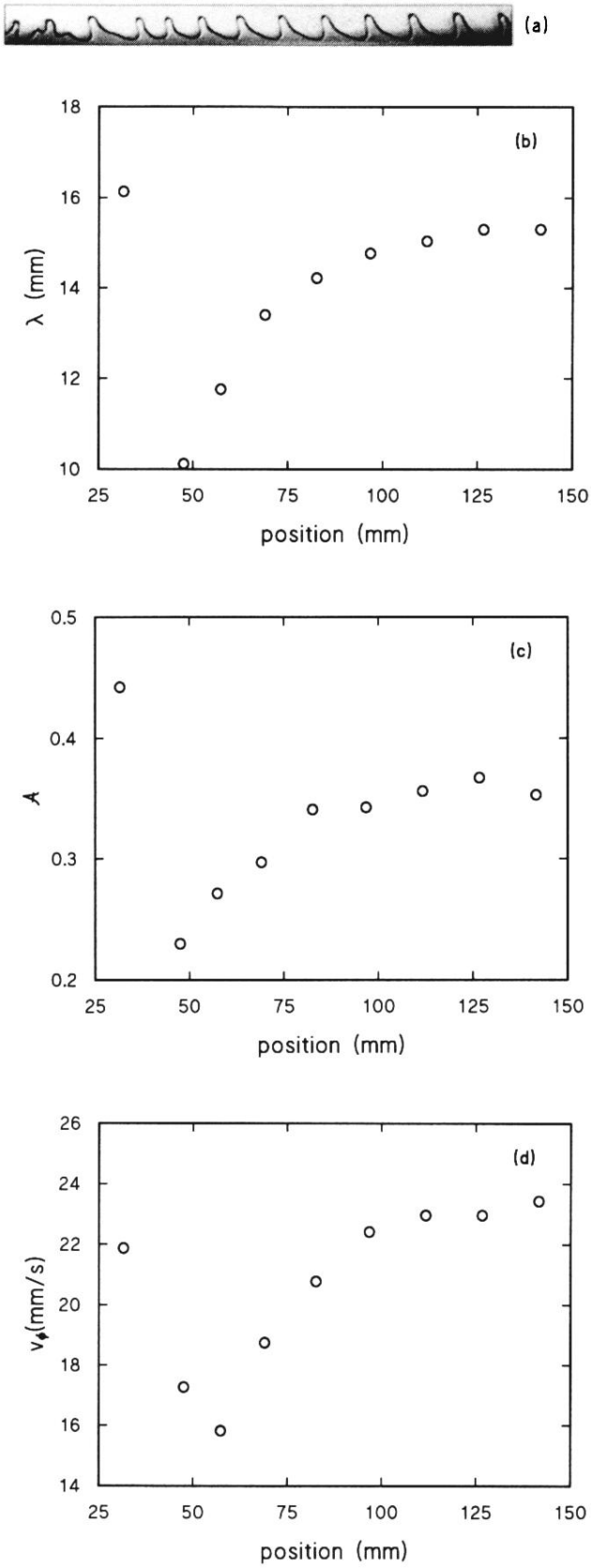

FIG. 4. The variation of the local properties of a nonuniform traveling pattern, as a function of position, for v_o = 261.4 mm/s, v_i = 55.42 mm/s. (a) The pattern itself. (b) The local wavelength, λ. (c) The asymmetry of the fingers, $\mathcal{A}$. (d) The local traveling speed, v_ϕ.

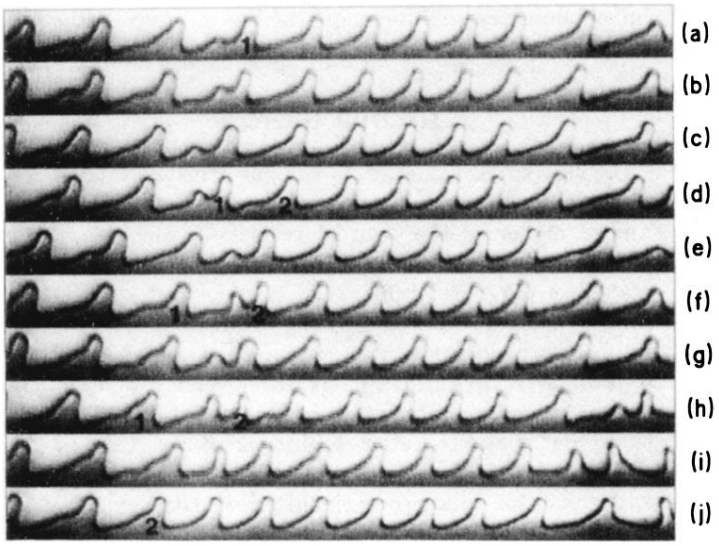

FIG. 9. The formation of a new finger when the local wavelength becomes too long. Here $v_o = 239.6$ mm/s and $v_i = 47.50$ mm/s. The images were recorded at times (a) 0 s; (b) 0.10 s; (c) 0.23 s; (d) 0.35 s; (e) 0.68 s; (f) 0.83 s; (g) 1.00 s; (h) 1.23 s; (i) 1.73 s; and (j) 2.73 s.